Journal of Petroleum Science and Engineering 193 (2020) 107349

Contents lists available at ScienceDirect

Journal of Petroleum Science and Engineering

journal homepage: www.elsevier.com/locate/petrol

Simulation study of water cut surge after CO_2 injection in tight oil reservoirs

Chi Zhang, Ye Tian *, Yizi Shen, Bowen Yao, Yu-Shu Wu

Petroleum Engineering Department, Colorado School of Mines, Golden, CO 80401, USA

ARTICLE INFO

Keywords:
CO_2 huff-n-puff
Enhanced oil recovery
Water cut
Compositional model
Tight oil
Hydraulic fracture

ABSTRACT

Tight oil contributed to 64% of total US oil production in 2019. However, recovery factors (RF) in tight oil reservoirs are low, typically less than 10% after primary depletion. Based on numerous published studies, gas huff-n-puff emerges as the most promising technique to push the RF beyond 10%. A recent pilot in the Wolfcamp shale confirmed the effectiveness of CO_2 huff-n-puff; however, an unexpected water cut surge was also observed during the puff stage. A compositional modeling framework was hence implemented to investigate the reasons as well as the impact of such phenomena. To the best of our knowledge, it is the first time that such abnormal water cut behavior has been modeled for tight oil reservoirs. The fluid PVT and lab-scale model were established and tuned to obtain the critical inputs for the compositional model. A half-stage model of five fractures was then established as a base case, representing a typical completion design in this region. Its results demonstrated an improved oil RF from 7.96% of depletion to 12.16% after six cycles of CO_2 huff-n-puff. And the improvement factor as 1.53 matched the published results of gas injection pilots in unconventional reservoirs. Based on the literature review, we found several possible mechanisms behind the water cut surge including underestimation of initial water saturation, interfacial tension (IFT) dependent relative permeability, reactivation of water-bearing layers, and re-opening of unpropped hydraulic fractures. Simulation-based sensitivity studies identified the re-opening of unpropped hydraulic fractures as the most plausible cause. The excessive water production was found to reduce the RF to 11.02% in contrast to a RF of 12.16% of the base case, marking the water management as a vital direction for future research.

1. Introduction

The commercial development of unconventional liquid-rich basins, such as Permian, has been a huge success due to the combination of horizontal well and multistage hydraulic fracturing. Tight oil produced from ultra-low permeability shale, sandstone, and carbonate formations contributed to approximately 64% of total U.S. crude oil production in 2019 (EIA, 2020). But smaller fracture spacings, or longer lateral lengths do not necessarily guarantee long-term success. In fact, the oil recovery factor (RF) is typically lower than 10% in most tight oil plays and a rapid decline in production rate is often very common (Sheng, 2015). Hence Improved/Enhanced Oil Recovery (IOR/EOR) in tight oil reservoirs has never been more important for operators.

Over the past decade, many technologies have been tested for IOR/EOR in tight oil reservoirs, among which the most promising one seems to be gas injection (injecting hydrocarbon gas, CO_2, N_2, etc.). Compared with water, gas has a much higher injectivity and could better supply reservoirs with additional energy. Gas could also lead to the swelling and viscosity reduction of oil. In addition, a reduced IFT in miscible injection often means more mobilized oil (Tang et al., 2019). Lastly, gas injection with hydrocarbon gas or CO_2 could reduce the environmental impact from gas flaring or greenhouse gas emissions (Wang et al., 2017). Gas huff-n-puff is often favored compared with flooding when reservoir permeability is lower than 0.1 mD (9.87×10^{-17} m^2), because of its shorter response time and the easiness as a single-well operation (Sheng, 2015). Among all of the gas sources, CO_2 is an ideal solvent owing to its capability of extracting intermediate hydrocarbon components, e.g., the natural gas liquid (Wang et al., 2017).

Early laboratory investigations (Kovscek et al., 2008; Vega et al., 2010) had revealed the potential of CO_2 injection in tight oil reservoirs. And the IOR/EOR mechanisms might include oil swelling, viscosity reduction, alternating rock wettability towards water-wet, reducing IFT between hydrocarbon-enriched CO_2 and CO_2-enriched oil (Hawthorne et al., 2013; Teklu, 2015). Subsequent studies also confirmed the viability of CO_2 huff-n-puff in the core scale by experiments (Wang et al., 2013; Tovar et al., 2014; Zhang, 2016; Jin et al., 2017; Song and Yang, 2017; Li et al., 2018, 2019) as well as its feasibility in the reservoir scale by simulation (Chen et al., 2014; Sanchez-Rivera et al., 2015; Yu et al., 2019; Sahni and Liu, 2018; Sun et al., 2019; Kerr et al., 2020). But the studies based on field observations are far from being enough or mature (Wang et al., 2017).

* Corresponding author.
E-mail address: yetian@mines.edu (Y. Tian).

https://doi.org/10.1016/j.petrol.2020.107349
Received 16 December 2019; Received in revised form 23 February 2020; Accepted 28 April 2020
Available online 5 May 2020
0920-4105/

1.1. Field observations

A CO_2 huff-n-puff pilot implemented in the Wolfcamp formation of the Midland Basin witnessed a significant oil rate improvement. But meanwhile, it recorded an unexpected water cut surge with an absolute value of around 0.3. To the best of our knowledge, this phenomenon has never been reported or explained in the related literature. To identify the cause of the water cut surge as well as manage the excessive water production after CO_2 injection in tight oil reservoirs, the related work in the literature needs to be reviewed.

Most published studies on gas IOR/EOR in unconventional reservoirs focused on the incremental oil recovery, but they paid less attention to the associated water production. Hoffman and Evans (2016) reviewed several IOR/EOR pilots in the Bakken, where gas huff-n-puff showed little improvement regarding oil rate and water production data was not mentioned. However, they reported a well which had neither oil nor water rate increase immediately after water huff-n-puff, but almost a year later it exhibited both increased oil rate and a water cut above 0.7. Hoffman (2018) summarized seven gas huff-n-puff pilots in the Eagle Ford and reported that gas injection would improve the cumulative oil production by 30%–70% in comparison to the depletion case. But no water production data were reported. Kerr et al. (2020) built a single porosity compositional model to match the primary production data of three Eagle Ford wells. The water cut of all wells declined initially and become steady within one year. For the subsequent gas huff-n-puff, it seems that water production was not a problem as water injection was even proposed in the edge wells to confine the injected gas. An important reason for little attention on water production is that water cut for the depletion stage is often quite stable except for an initial spike, which is largely due to the flowback of fracturing fluids (Pankaj et al., 2018). Though rarely, water cut would sometimes surge if the induced fractures invaded other zones, such as the overlaying Lodgepole formation in the Bakken play (Jin et al., 2017) or the Bone Spring formation in the Delaware basin (Muirhead and Pettit, 2016). Specifically, for the Wolfcamp formation of Delaware basin, Muirhead and Pettit (2016) classified the water cut behaviors into three categories: (a) High water cut with an average value of 0.8. (b) Medium water cut with an average value of 0.4. (c) Low to high water cut, well exhibiting water cut 0.2–0.4 at first, but then a surge to 0.9 within 6 months. Their simulation model concluded that it was the hydraulic fractures propagating from the Wolfcamp into the Bone Spring formation that caused the rising water cut, revealing the fracture height as a critical factor contributing to the excessive water production during depletion. Unfortunately, little water production data is available for huff-n-puff operations in liquid-rich shale.

Water production data is more accessible in conventional, high permeability reservoirs, but the water cut is often observed as unchanged or even reduced after gas injection, especially for immiscible projects. Hsu and Brugman (1986) reported an immiscible CO_2 huff-n-puff pilot in the Paradis field, Louisana. The pre-injection water cut was 0.9, and the average water cuts for the first and second cycle were almost unchanged. Denoyelle and Lemonnier (1987) reported a stripper well case in a shallow sandstone reservoir with permeability in the range 5–20 mD ($4.93–19.7 \times 10^{-15}$ m^2) and in-situ oil viscosity as 2.68 cP. Though not explicitly mentioned, the project was likely immiscible as a black oil simulator was used. Before CO_2 injection, one well produced at 2 STB/day with water cut as 0.9. After CO_2 injection, water cut first decreased, and then bounced back to 0.9. Haskin and Alston (1989) evaluated 28 immiscible CO_2 huff-n-puff projects in Miocene reservoirs and found that water rates would generally decrease with increased oil rate after injection, but finally water cut would return to the pre-injection value. Monger and Coma (1988) summarized nine successful pilots in the South Louisiana oil-bearing sands. Eight of the wells experienced water cut reduction after CO_2 injection. Only one well, Well J, experienced a water cut surge from 0.30 to 0.67 after injection. Unlike the other eight wells, this well was apparently injecting above the MMP (Minimum Miscibility Pressure). Hence achieving miscibility might be another vital factor for the water cut surge.

Monger et al. (1991) reported an immiscible CO_2 huff-n-puff in the Appalachian Basin in Eastern Kentucky. Sixty-five wells were tested in a fractured reservoir with average permeability as 10 mD (9.87×10^{-15} m^2). The author compared water cut data before and after CO_2 injection and proposed that water was pushed away by injected CO_2, leading to a reduced water cut. For the viscous oil, there was even a patented technology, called the Anti-Water Coning Technology (AWACT), which involves injecting immiscible gas into a watered-out well to suppress water conning (Luhning et al., 1990). AWACT succeeded in 40 wells in the South Jenner oilfield (Lai and Wardlaw, 1999) with the in-situ viscosity as 97 cP. The reduced water cut and improved oil recovery were attributed to the trapped gas which lowered the relative permeability to water and redirected the water influx. Mohammed-Singh et al. (2006) reviewed 16 CO_2 huff-n-puff projects in the Forest Reserve oilfield of Trinidad and Tobago. Projects were successful in reservoirs with in-situ oil viscosities from 0.5 to 3000 cP and permeabilities ranging from 10 (9.87×10^{-15} m^2) to 2500 mD (2.47×10^{-12} m^2). They concluded that CO_2 injection could reduce the relative permeability to water due to trapped gas saturation and oil swelling. Hence redistribution of fluid saturation and the resulting relative permeability alteration due to injection might also be an influential factor.

Simpson (1988) reported two immiscible CO_2 huff-n-puff tests in a bottom-water reservoir with water cut between 0.98 and 0.99, caused by water coning. Though both tests witnessed incremental oil production, the water cut responses were very different. For Well 271, the water cut was as low as 0.002 once the puff started. Then within five days, the water cut increased to 0.57; but it remained between 0.7 and 0.8 for almost two months. Finally, it went back to the pre-test value as 0.99 in 100 days. For Well 272, once the puff started, the water cut was continuously decreasing from 1 to 0.78, and it rose again back to 0.92. Then the well was shut-in again for two months, and water cut again decreased to 0.76, but gradually returned to the pre-test value as 0.99 in 50 days. Well 271 was shut-in for 51 days in contrast to the 28 days of Well 272. Moreover, Well 271 received 18% more CO_2 than Well 272 within the 5-day injection time. Operational parameters such as shut-in time and injected gas volume may contribute to the different water cut responses.

1.2. Laboratory studies

Many lab-scale investigations of CO_2 injection have been performed on low-permeability cores, but most of them focused on the improved oil recovery. Very few of them contemplated initial water saturation (Tovar et al., 2014; Jin et al., 2017; Song and Yang, 2017; Li et al., 2018), let alone the production of water. Tovar et al. (2014) investigated CO_2 huff-n-puff in preserved shale samples of nD permeability with packed glass beads simulating fractures. Their work confirmed the incremental RF but observed no water production even with initial water saturation estimated as 0.3. Li et al. (2018) investigated the effect of water on CO_2 huff-n-puff performance and found that RF would decrease by 45% with an initial Sw as 0.4 in contrast to cores without water. Water cut though not explicitly plotted was increasing with time.

CO_2 injection related water data is also very limited even in cores from conventional reservoirs. Darvish et al. (2006) investigated the efficiency of immiscible CO_2 injection into fractured cores with permeability of 4 mD (3.95×10^{-15} m^2). CO_2 was injected to displace the residual oil in a water-flooded core. The results indicated that the water production rate was around ten times higher than the oil rate at first, but it decreased to zero after several days. The author concluded that the high-water cut was the result of high initial water saturation in the core. Torabi and Asghari (2010) examined the performance and efficiency of cyclic CO_2 injection in the fractured porous media. Two Berea cores were tested with matrix permeability as 100 mD (9.87×10^{-14} m^2) and 1000 mD (9.87×10^{-13} m^2), respectively. The cylindrical core was held in a steel cell with 0.5 cm (5×10^{-3} m) annular spacing to simulate the matrix and its surrounding fracture in this set-up. The results suggested that the connate water existence would favor RF during immiscible CO_2 huff-n-puff processes, but there was no obvious difference in RF under miscible conditions. Abedini and Torabi (2014) investigated CO_2 huff and puff in cores with permeability around 70 mD (6.91×10^{-14} m^2) and connate water saturation ranging from 0.443 to 0.459. Their experimental results indicated that no water production was found after CO_2 injection even for cases above MMP.

In summary, the initial water cut spike during the depletion of liquid-rich unconventional reservoirs is largely due to the flowback of fracturing fluids. Fracture propagation into adjacent water layers is a possible reason for the water cut increase after flowback. For conventional reservoirs, gas injection rarely results in water cut increase, even for watered-out wells except one case when injection was miscible. Fluid saturation redistribution and a further shifted relative permeability might also be an important factor. The operational parameters, such as shut-in time or injected volume may also affect the behavior of the water cut. Experimental studies of gas huff-n-puff in cores have shown contradicting roles of initial water saturation on oil RF, but initial water saturation is a decisive factor worth exploring during gas huff-n-puff. We hence plan to investigate the above-mentioned relevant factors with a compositional model, whose key inputs including fluid characterization, pore compressibility and relative permeability curves were all based on the related laboratory studies.

2. Matching experimental data

The results of PVT measurements and core experiments were matched first to provide critical inputs for the reservoir-scale model.

2.1. Reservoir fluid characterization

The composition of a typical oil sample from Wolfcamp shale has been analyzed up to C_{36+} by a third-party laboratory. In this study, a fluid model was established based on the Peng-Robinson (PR) equation of state (EOS) with eight components, i.e., C_1, CO_2, N_2–C_2, C_3, C_4–C_6, C_7–C_{15}, C_{16}–C_{24}, and C_{25+}. Their thermodynamic properties were tuned to match the various experiment results, including the constant composition expansion (CCE), differential liberation, swelling test, and viscosity measurement. Since CH_4 will also be used as injectant in the future work, it was deliberately not lumped together with N_2. C_3 was listed as an individual component to represent the improved recovery of natural gas liquids (NGL). N_2 was lumped with C_2, because the operator do not plan to inject either pure N_2 due to its low efficiency or pure C_3 due to its high cost. Besides, N_2 only has a molar fraction of 0.24%, which would lead to negligible effects on thermodynamic properties when lumping with C_2. Following a proper tuning procedure (Pan et al., 2015), the calculated curves after regression by WinProp satisfactorily matched the experimental data, as shown in Figs. 1–4. The thermodynamic properties for each component after tuning were summarized in Table 1 and the binary interaction coefficients between any two components were summarized in Table 2.

PR EOS was used to calculate the oil properties at the reservoir temperature of 170 °F (349.8 K), and estimated the saturation pressure as 2263.7 psi (1.56×10^7 Pa), oil gravity as 43 °API (810.89 kg/m^3), formation volume factor as 1.38 RB/STB and GOR as 780 SCF/STB (138.92 m^3/m^3). The minimum miscibility pressure (MMP) between the reservoir oil and injected CO_2 was estimated as 3064.5 psi (2.11×10^7 Pa) by the multiple mixing cell method. The stock tank oil and produced gas composition were summarized in Table 3.

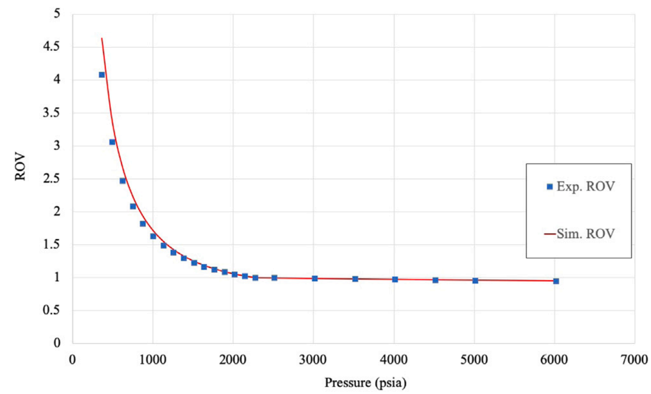

Fig. 1. Matching the relative volume (ROV) from the CCE test.

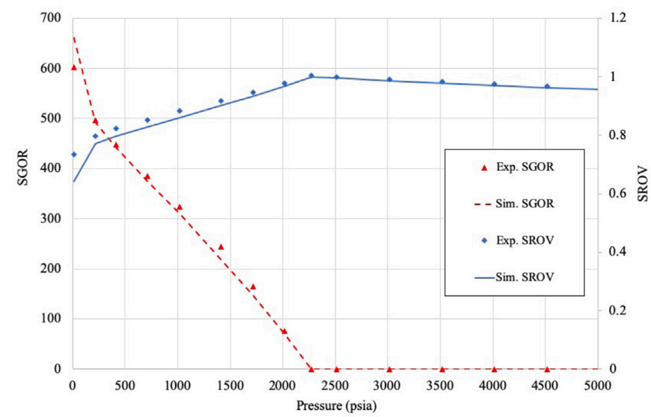

Fig. 2. Matching the results of differential liberation test.

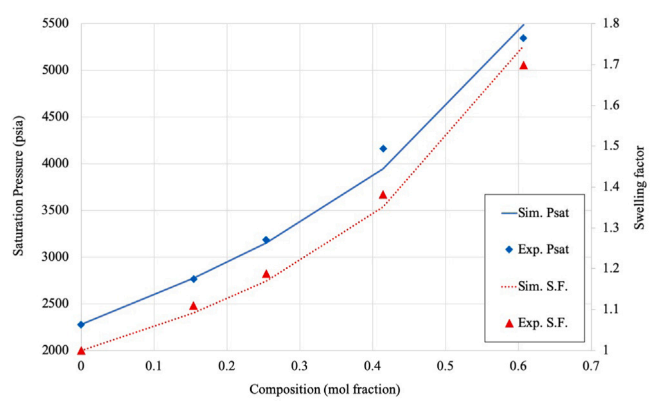

Fig. 3. Matching the results of swelling test with the produced gas.

2.2. Simulation model for huff-n-puff experiment in a composite core

Gas huff-n-puff tests were designed and conducted by our industry partner in a composite core, consisting of a low permeability plug and a high permeability plug, as shown in Fig. 5. Lab-scale modeling was then implemented to fit the experimental data provided by our industry partner. The composite core consists of two plugs as shown in Fig. 5. The underlying Wolfcamp shale core has a diameter of 2.11 inch (5.36×10^{-2} m) and a length of 2.57 inch (6.53×10^{-2} m). The porosity is 0.082 and the permeability is 0.11 mD. A high permeability Berea sandstone core disk ($k = 2200$ mD, $\phi = 0.224$), which has a diameter of 2.11 (5.36×10^{-2} m) inch and a length of 0.25 inch (0.64×10^{-2} m) is

Table 1
Thermodynamic properties of each component after tuning.

Component	Molar fraction	Pc, atm	Tc, K	Vc, L/mol	Acentric factor	MW, g/mol	Vol. Shift
CO_2	0.0048	72.8	304.2	0.094	0.225	44.0	0
CH_4	0.3517	45.4	190.6	0.099	0.008	16.0	0
N_2–C_2	0.0972	48.1	301.2	0.146	0.097	30.0	0
C_3	0.0801	41.9	369.8	0.203	0.152	44.1	0
C_4–C_6	0.1173	34.8	457.4	0.292	0.226	69.2	0
C_7–C_{15}	0.2400	25.4	581.6	0.510	0.402	138.1	0.042
C_{16}–C_{24}	0.0592	21.3	828.1	0.983	0.765	259.5	−0.154
C_{25+}	0.0496	10.6	987.8	1.483	0.875	377.6	0.263

Table 2
Binary interaction coefficients after tuning.

Component	CO_2	CH_4	N_2–C_2	C_3	C_4–C_6	C_7–C_{15}	C_{16}–C_{24}	C_{25+}
CO_2	0	0.08	0.08	0.1	0.06	0.06	0.05	0.05
CH_4	0.08	0	1.714E−3	5.744E−3	1.383E−2	3.126E−2	5.976E−2	8.139E−2
N_2–C_2	0.08	1.714E−3	0	1.193E−3	5.297E−3	1.712E−2	3.910E−2	5.682E−2
C_3	0.1	5.744E−3	1.193E−3	0	1.474E−3	9.392E−3	2.714E−2	4.250E−2
C_4–C_6	0.06	1.383E−2	5.297E−3	1.474E−3	0	3.465E−3	1.627E−2	2.880E−2
C_7–C_{15}	0.06	3.126E−2	1.712E−2	9.392E−3	3.465E−3	0	4.816E−3	1.263E−2
C_{16}–C_{24}	0.05	5.976E−2	3.910E−2	2.714E−2	1.627E−2	4.816E−3	0	1.888E−3
C_{25+}	0.05	8.139E−2	5.682E−2	4.250E−2	2.880E−2	1.263E−2	1.888E−3	0

Table 3
Composition of the produced gas and stock tank oil.

Component	Produced gas	Stock tank oil
CO_2	0.0080	0.0004
CH_4	0.7067	0.0011
N_2–C_2	0.1632	0.0063
C_3	0.0882	0.0353
C_4–C_6	0.0333	0.1947
C_7–C_{15}	0.0006	0.5241
C_{16}–C_{24}	0	0.1295
C_{25+}	0	0.1085

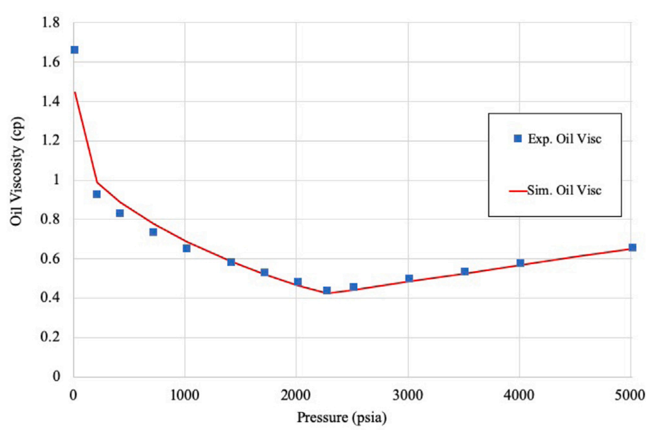

Fig. 4. Matching the results of oil viscosity measurement.

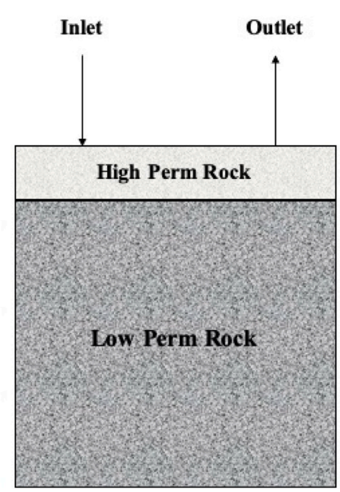

Fig. 5. Schematic of the composite core used in the gas huff-n-puff experiments.

stacked at the top shale core to represent a hydraulic fracture. In this study, we mainly focus on the modeling perspective to understand the reason behind the surging water cut, and more details on the laboratory investigation could be found in Tang et al. (2016).

Before the experiment, the core sample was cleaned and dried to remove any remaining hydrocarbons, water, and brine. Then the cores were sequentially flooded by synthetic formation brine and the stock tank oil (composition shown in Table 3) to establish the initial oil saturation as 0.5 and pressure as 4000 psi (2.76×10^7 Pa). A constant temperature of 170 °F (349.8 K) and a confining pressure of 4500 psi (3.10×10^7 Pa) was maintained in the core holder through each run. The system was first depleted to 600 psi (4.14×10^6 Pa) to simulate the primary production before the gas injection. Gas (CH_4) was then injected from the top and pressurized the system to 4000 psi (2.76×10^7 Pa). The system was subsequently closed to simulate soaking processes and was depleted again to 600 psi (4.14×10^6 Pa), representing the puff stage. The production stage stopped when no additional fluid could be produced. The detailed starting time of each stage was shown in Table 4. The produced fluids were then separated but only water and oil were collected and measured respectively at the standard condition.

We then used a lab-scale cylindrical model to match the results of huff-n-puff experiments in the composite core. There were 10 grids in the radial direction and 6 grids in the axial direction, as shown in

Table 4
Operating procedure of the huff-n-puff experiments.

Stage	Time, min	Operating pressure, psi
Initial	0	4000
Depletion	51	600
Injection	60	4000
Soaking	2610	4000
Production	2700	600
Injection	2705	4000
Soaking	8400	4000
Production	8457	600
Injection	8462	4000
Soaking	18227	4000
Production	18417	600

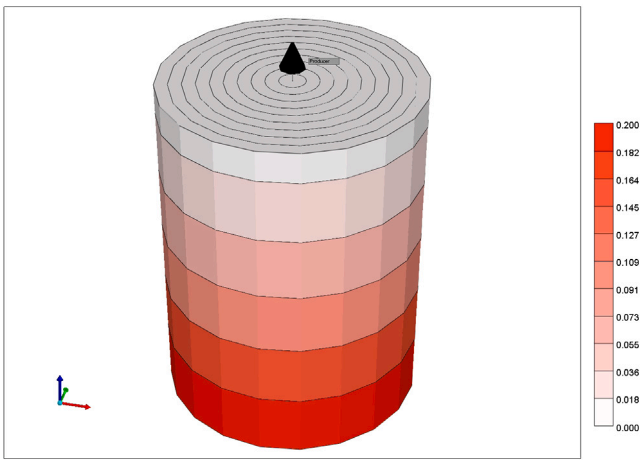

Fig. 6. Lab-scale model for gas huff-n-puff in the composite core.

Fig. 6. The fluid model established earlier was used in this lab-scale compositional model.

History matching of the experimental results was then completed. Since the BHP (bottom hole pressure) was set as the history matching constraint, its values were exactly the same as the experimental data. Relative permeability curves of the low permeability rock representing matrix were tuned primarily to match the cumulative oil and water production as shown in Fig. 7. Though the water-oil ratio is lower than the value observed in the field, the water production was not zero unlike many previous huff-n-puff experiments (Tovar et al., 2014; Abedini and Torabi, 2014) in tight cores.

The relative permeability curves for high permeability rock representing fractures were generated as straight lines by assuming negligible capillary pressures. The final relative permeability curves that led to the best match are shown in Figs. 8 and 9. Matrix rock compressibility was also found important in the matching process and a final value of 5×10^{-6} psi^{-1} (7.25×10^{-10} Pa^{-1}) was found to provide the best match. Please note that the original experiment used CH_4 as the injected gas, but the water-oil relative permeability curves should hold regardless of the gas species. It was also assumed that the gas-liquid relative permeability curve was identical for CH_4 and CO_2.

3. Simulation base case

A typical horizontal producer in this region has a perforated lateral of 10,000 ft (3.05×10^3 m) with 100 fracturing stages. Propped and unpropped hydraulic fracture, enhanced permeability region, and natural fracture and matrix were taken into consideration in the model, as shown in Fig. 10. There are five perforation clusters in each stage, which are assumed identical to each other and uniformly distributed over the lateral as shown in Fig. 11. The dual permeability model was used to capture natural fracture networks. Within a hydraulic fracture, it is assumed that the fracture tip region is unpropped and hence has a smaller conductivity (blue region in Fig. 11). The hydraulic fracture half-length is 390 ft (118.9 m) and the propped length (red and yellow region in Fig. 11) is 147 ft (44.8 m).

The dimension of the model in I direction is 100 ft (30.5 m) to cover a single fracturing stage. Since the distance between two parallel horizontal wells in J direction is set to be 880 ft (268.2 m), by assuming

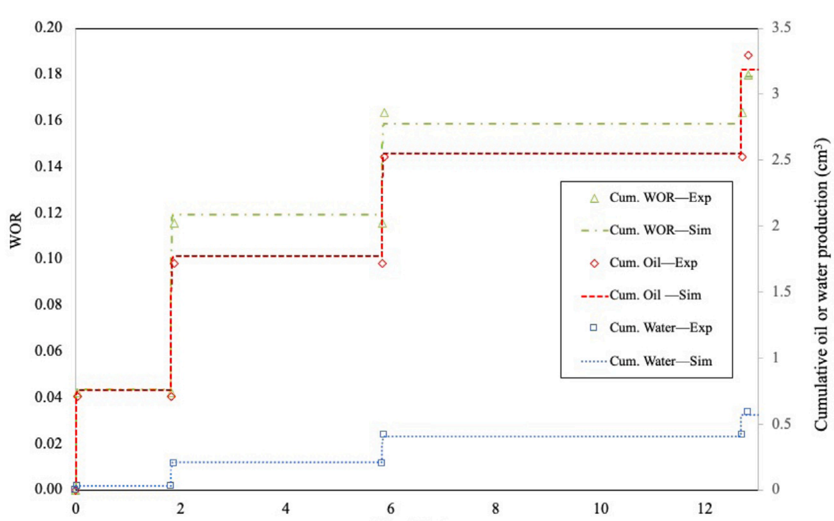

Fig. 7. Matching the results of huff-n-puff experiments in the composite core.

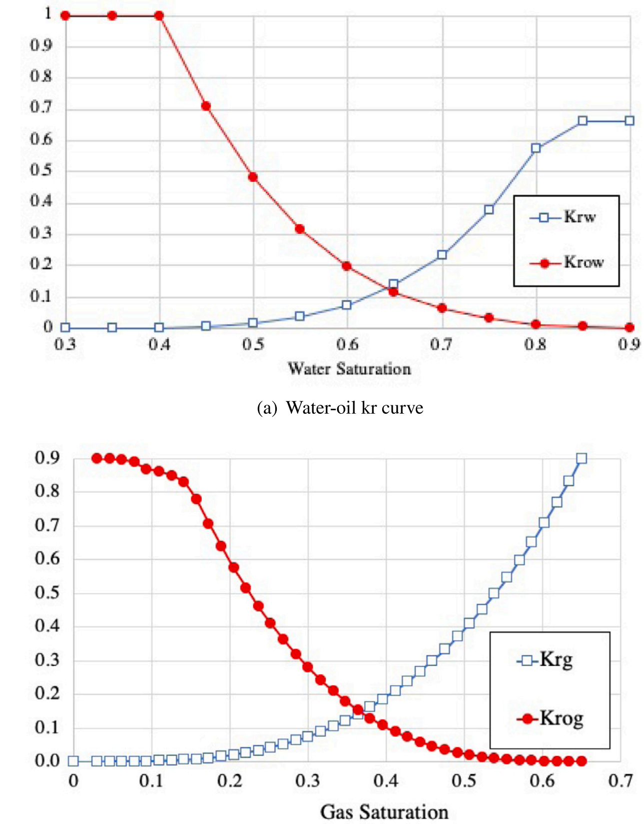

(a) Water-oil kr curve

(b) Liquid-gas kr curve

Fig. 8. Matrix relative permeability curves after history matching.

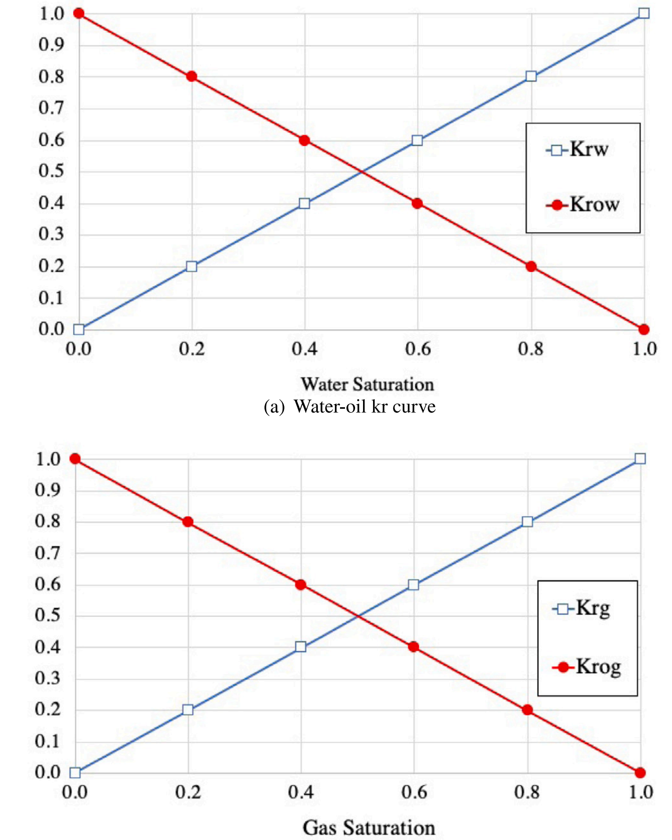

(a) Water-oil kr curve

(b) Liquid-gas kr curve

Fig. 9. Fracture relative permeability curves after history matching.

they are identical, a closed flow boundary can then be established by symmetry. Therefore, the whole stage can be simplified with a half-stage model with a dimension as 440 ft (134.1 m) in the J direction. In the K direction, there is no symmetry hence the entire formation is modeled with all 15 layers. The simplification using symmetry was commonly used in other work (Brown et al., 2011; Tian et al., 2019). Table 5 summarizes the geometry of the half-stage model with five planar fractures. It is worth mentioning that the "stage" in our model is a half-stage by assuming a mirror plane perpendicular to the J direction as shown in Fig. 10 and Fig. 11, hence a factor of 200 should be used to scale any production or injection rates for a well with 100 full stages.

For the primary mesh before refinement, there are 35 grids in the I-direction, 15 grids in the J direction, and 15 grids in the K direction corresponding with 15 vertical layers. Then the hydraulic fractures were created with a planar fracture template and refined grids were used near the fracture which made the total grid number 14,625. The grid system of the conceptual model after refinement was shown in Fig. 12.

For the fracture grid, it is assumed that the effective porosity of natural fracture is 0.0001 and the effective horizontal permeability is 0.025 mD (2.47×10^{-17} m^2). For the matrix grid block, it is assumed that rock properties including porosity, horizontal permeability, and initial water saturation only vary vertically and within each layer they are all homogeneous. The matrix properties of different layers are summarized in Table 6 and were provided by our industry partner. For both matrix and fracture, vertical permeability is assumed to be 1/10 of the horizontal permeability. The natural fracture spacing is 50 ft (15.24 m) in the I and J direction and 0 ft (0 m) in the K direction.

Since the hydraulic fracture (HF) is modeled explicitly by locally refined grids, and the grid width w_{grid} containing HF as 0.1 ft (3.05×10^{-2} m) is much larger than the actual width of HF, w_{HF} as 0.001 ft ($3.05 \times$

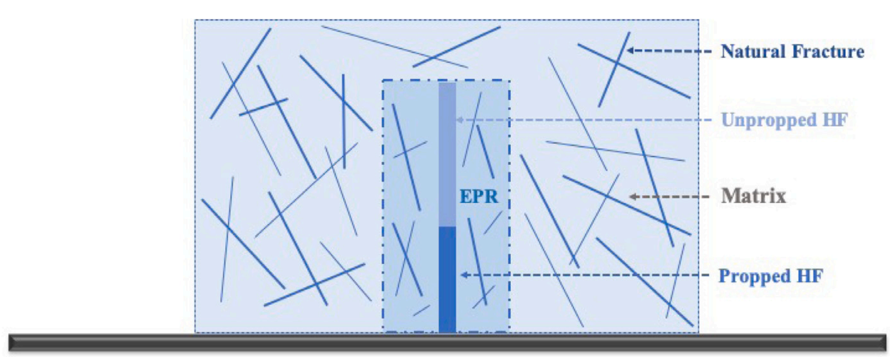

Fig. 10. Schematic of the half-stage model in the I-J plane.

Table 5
Geometry of the base case for reservoir simulation.

Well geometry		Model dimension	
Perforated lateral length, ft	10000	X in I-direction, ft	100
Stage number	100	Y in J-direction, ft	440
Clusters per stage	5	Z in K-direction, ft	236
Cluster spacing, ft	20	Fracture half-length, ft	390

Table 6
Rock properties of the matrix grid at different layers.

Layer	Thickness, ft	Porosity	Permeability, mD	Initial water saturation
1	10	0.0661	2.046×10^{-4}	0.57
2	30	0.0581	1.271×10^{-4}	0.68
3	24	0.1037	1.101×10^{-3}	0.36
4	18	0.0713	2.720×10^{-4}	0.36
5	13	0.0617	1.591×10^{-4}	0.65
6	17	0.0598	1.409×10^{-4}	0.70
7	13	0.0677	2.240×10^{-4}	0.59
8	17	0.0590	1.346×10^{-4}	0.66
9	15	0.0499	7.171×10^{-5}	0.84
10	13	0.0502	7.371×10^{-5}	0.94
11	12	0.0362	2.171×10^{-5}	1.00
12	15	0.0338	1.686×10^{-5}	0.81
13	15	0.0882	6.020×10^{-4}	0.70
14	10	0.0439	4.457×10^{-5}	0.63
15	14	0.0763	3.509×10^{-4}	0.53

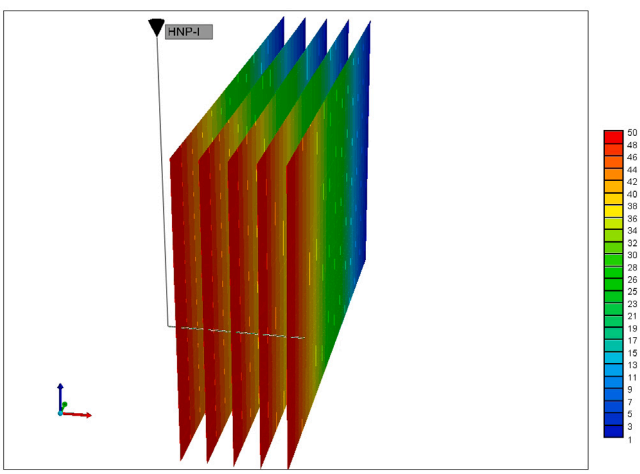

Fig. 11. Realization of the conceptual half-stage model in CMG. (For interpretation of the references to colour in this figure legend, the reader is referred to the web version of this article.)

10^{-4} m). The grid effective permeability k_{HFeff} is scaled accordingly to maintain the same fracture conductivity as specified (CMG, 2018).

$$k_{HFeff} = \frac{k_{HF} w_{HF}}{w_{grid}} \tag{1}$$

For example, the grid block effective permeability for the propped HF is 50 mD (4.93×10^{-14} m^2), which is the propped HF's conductivity (5 mD·ft, 1.5×10^{-15} m^3) divided by the grid width (0.1 ft, 3.05×10^{-2} m). The stress-dependency of fracture permeability is modeled using a compaction table. The unpropped HF and natural fracture (NF) are assumed to follow the same trend, while propped HF should follow a different curve with a weaker dependency on stress and a higher remaining permeability as shown in Fig. 13.

The initial reservoir pressure was 4687 psi (3.23×10^{7} Pa) and the temperature was 170 °F (349.8 K) at the mid-depth of the reservoir. In order to capture the water cut spike during the flowback, water was first injected with a total volume as 2320 STB (368.85 m^3) to simulate a typical fracturing job in this region. The half-stage was first depleted for four years with a maximum oil rate as 10 STB/day (1.84×10^{-5} m^3/s) and a minimum BHP set as 1200 psi (8.27×10^{6} Pa). Then the well was injected with a maximum CO_2 rate of 6000 SCF/day (1.97×10^{-3} m^3/s) and maximum BHP of 7000 psi (4.83×10^{7} Pa) for 50 days. Shut-in time was set as 10 days. In the puff stage, the well was set to produce with a maximum oil rate of 10 STB/day and minimum BHP of 1200 psi (8.27×10^{6} Pa) for 300 days. The time duration of each stage in huff-n-puff was designed based on the actual field practice.

4. Results and discussions

A sensitivity study based on compositional simulation was conducted to identify the main mechanisms behind the abnormal water-cut responses as well as quantify the impacts of the associated water production during CO_2 huff-n-puff.

4.1. Huff-n-puff vs. depletion

The base model was established with six CO_2 huff-n-puff cycles simulated. A case with only depletion was also run as shown in Fig. 14. The recovery factor for the huff-n-puff base case was 12.16%, which was 1.53 times the RF of depletion as 7.96%. The improvement factor of 1.53 matched the field observations in the literature (Wang et al., 2017; Hoffman, 2018).

Table 7 shows the cumulative production of C_3 in moles. After gas injection, slightly less C_3 was recovered from the oil phase. However, a significant increase of C_3 production was observed in the produced gas, demonstrating an increased yield of NGL and the enrichment of the produced gas due to the vaporizing effect.

C_{7-15} is the main component of stock tank oil as shown in Table 3. After gas injection, its incremental production was mostly contributed by the increased production of oil phase as shown in Table 8, which to some extent could be related to the oil swelling and viscosity reduction effect.

We also analyzed the changing composition of the produced fluid over time. Before CO_2 injection (10/2021), the composition of produced oil was quite stable as shown in Fig. 15. Once CO_2 huff-n-puff started, the produced oil phase would contain fewer light (labeled as others in Fig. 15) or intermediate components (C_{4-6}) but more heavy components (C_{7+}). Compared with the oil composition of primary depletion, the produced oil composition was heavier at the early time of each puff stage, but it would gradually return to the initial oil

Table 7
Cumulative production of C_3.

	Produced C_3 in Oil, mol	Produced C_3 in gas, mol	Total C_3 produced, mol	C_3 RF
Depletion	81,867	312,133	394,000	7.06%
Huff-n-puff	81,036	543,200	624,237	11.18%

Table 8
Cumulative production of C_{7-15}.

	Produced C_{7-15} in Oil, mol	Produced C_{7-15} in gas, mol	Total C_{7-15} produced, mol	C_{7-15} RF
Depletion	1,129,557	5,389	1,134,945	7.93%
Huff-n-puff	1,770,180	24,539	1,794,719	12.54%

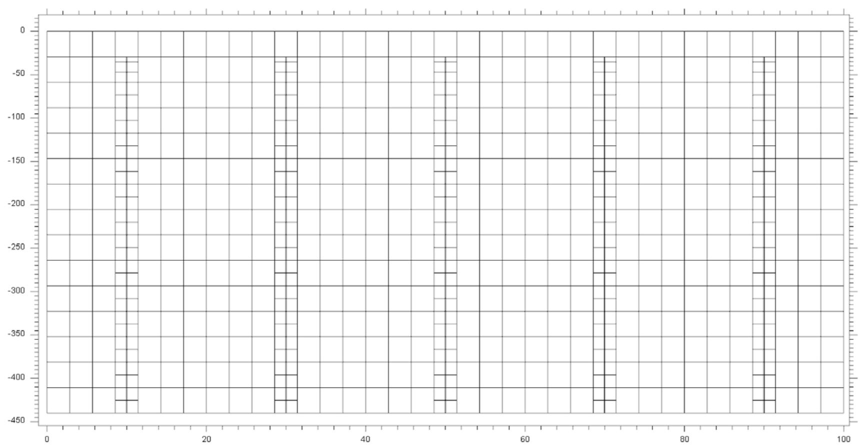

Fig. 12. The grid system in the I-J plane for the base case.

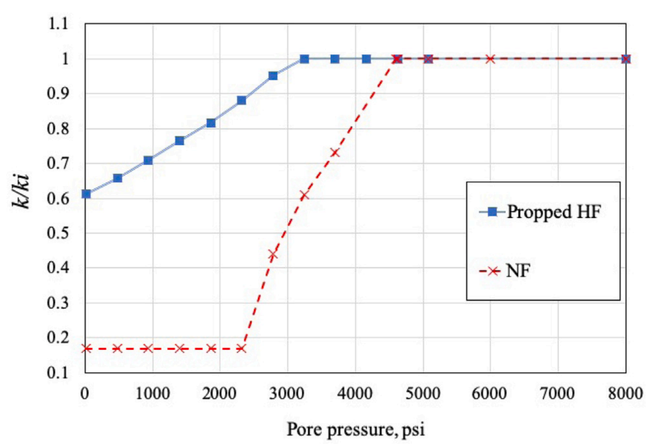

Fig. 13. Stress-dependent permeability correlation used in this study.

composition similar to that of primary depletion at the late time. This was mainly because the light or intermediate components were vaporized and produced with the injected gas.

For the gas phase composition as shown in Fig. 16, CO_2 would have the highest mole fraction once the huff-n-puff started. The mole fraction of any other component in the gas phase was reduced. But overall CO_2 huff-n-puff could still improve the RF of the light and intermediate components (e.g., improved C_3 production shown in Table 7), because the reduced mole fraction of light and intermediate components was compensated by the increased production of the gas phase after CO_2 injection.

With respect to the water cut, it initially reached a peak at 1.0 due to flowback, then it fell and remained almost constant as 0.39 which represented a typical water cut behavior during depletion. For huff-n-puff, the water cut would start at a very low value, as only CO_2 was being produced when the well was first opened. It then would reach a peak of 0.47 in around 250 days and then fell slightly after the peak. Finally, it would bounce back to a plateau as 0.44 and remain constant for the rest of the puff stage. With more cycles, the peak would gradually decrease but remain at a level still higher than the primary depletion as shown in Fig. 17.

Interestingly, the simulated water cut response somehow resembles that of Well 271 which is a CO_2 huff-n-puff in a conventional reservoir (Simpson, 1988) as shown in Fig. 18. But it is different from what was observed in the CO_2 pilots for the Wolfcamp formation. The observation from the Wolfcamp formation of Midland shows that the water cut will increase by an absolute value of around 0.3 from the depletion basis. It will slightly decrease at the early time of each cycle but remain at a level still higher than the depletion. Hence, we hereinafter explore several possible reasons behind such abnormal water cut response.

4.2. Possible reasons for the water cut surge

4.2.1. Initial water saturation

First, we assumed there were errors in the estimation of initial water saturation, and hence raised the initial water saturation S_{wi} of each layer by 10%. A value of 1 was used if the new initial water saturation of a layer exceeded one. The new water cut showed approximately a translation of 0.1 in the vertical axis based on the previous curve as shown in Fig. 19. But the trend still could not match the field observation as the water cut of primary depletion also witness an increase of 0.1. Though initial water saturation could potentially impact water production, it might not be the main reason behind the above-mentioned abnormal water cut behaviors after huff-n-puff.

4.2.2. IFT-dependent relative permeability

Often, researchers tend to neglect the effect of interfacial tension (IFT) on relative permeability (CMG, 2018) though it is a very

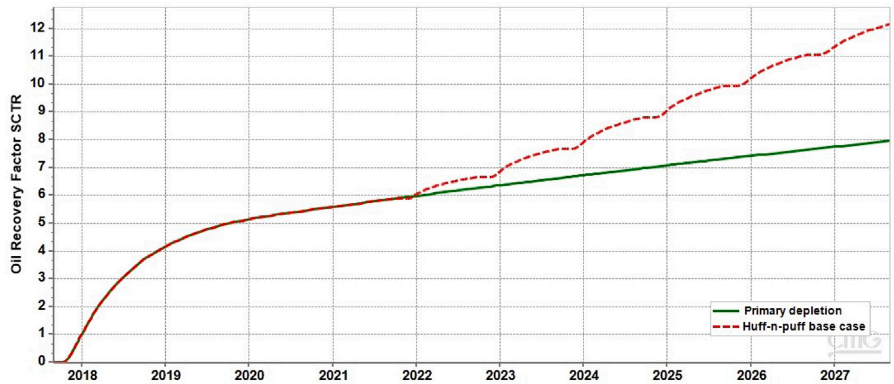

Fig. 14. Comparison of the oil RF between huff-n-puff and depletion.

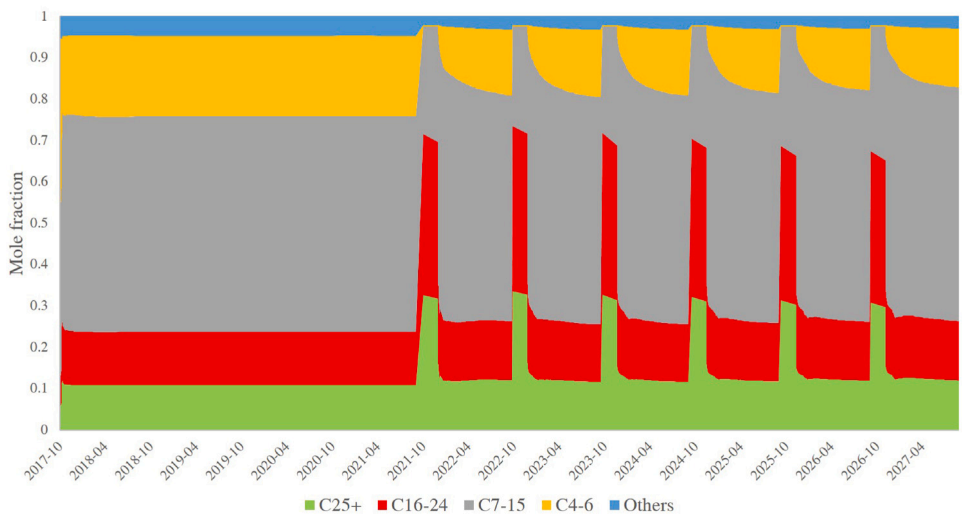

Fig. 15. Changing composition of the produced oil over time in the huff-n-puff base case.

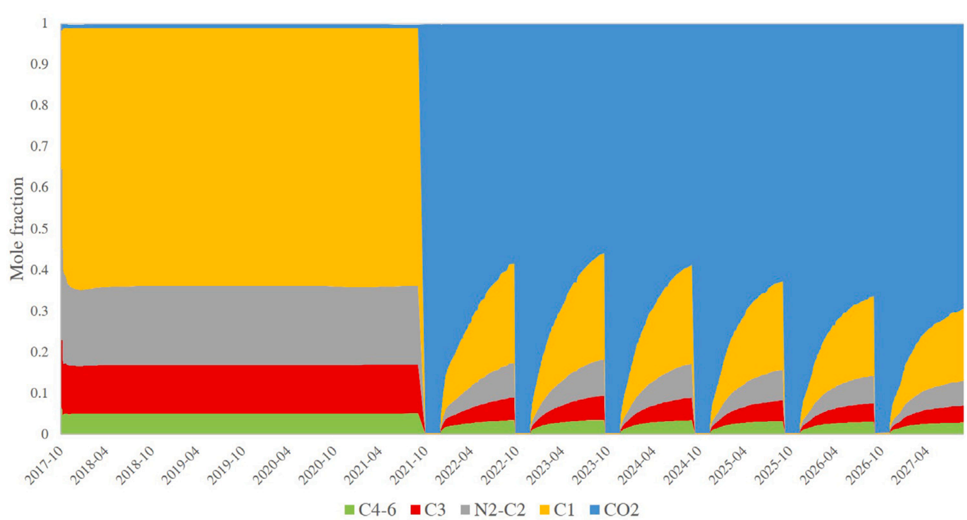

Fig. 16. Changing composition of the produced gas over time in the huff-n-puff base case.

important mechanism for the dynamics between immiscible and miscible displacement, which is the case in this study. The simulator (CMG-GEM) used in this study has an option of interpolating relative permeability curves as a function of IFT. The relative permeability curves for gas and oil will become linear functions of the respective saturations when the phases become nearly indistinguishable (as the IFT between oil and gas phase σ_{og} approaches zero).

$$k_{rot} = f(\sigma_{og})k_{ro}(S_w, S_g) + \left[1 - f(\sigma_{og})\right] k_{rhw}(S_w)\frac{S_o}{1 - S_w} \tag{2}$$

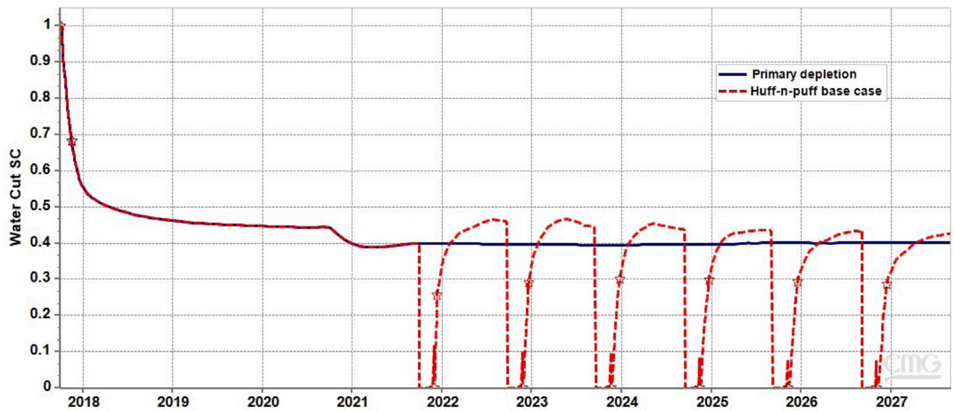

Fig. 17. Comparison of huff-n-puff and depletion water cut.

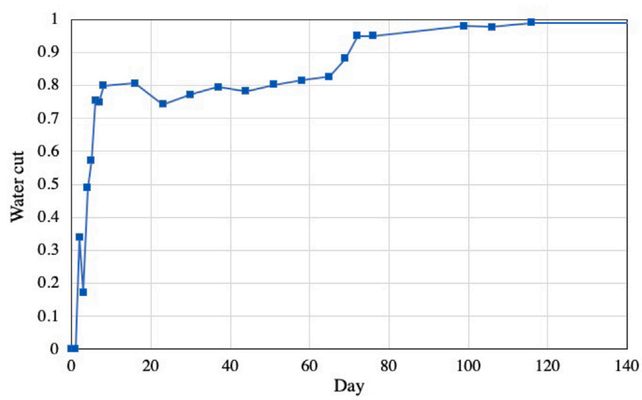

Fig. 18. Water cut response of CO_2 huff-n-puff in a conventional reservoir, modified based on Simpson (1988).

$$k_{rgt} = f(\sigma_{og}) k_{rg}(S_w, S_g) + \left[1 - f(\sigma_{og})\right] k_{rhw}(S_w) \frac{S_g}{1 - S_w} \tag{3}$$

$$k_{rhw}(S_w) = 0.5 k_{row}(S_w) + 0.5 k_{rlg}(S_w) \tag{4}$$

where S_w, S_o, S_g are the saturation of water, oil and gas phase respectively. k_{row}, k_{rlg} are water and gas relative permeability of the input relative permeability curve; k_{ro}, k_{rg} are oil and gas relative permeability before interpolation; k_{rot}, k_{rgt} are the oil and gas relative permeability after interpolation; And f is a piecewise function of σ_{og} as,

$$f(\sigma_{og}) = \begin{cases} 1, \ \sigma_{og} > \sigma_0 \\ \left(\sigma_{og}/\sigma_0\right)^n, \ \sigma_{og} \leqslant \sigma_0 \end{cases}$$

where σ_0 is a threshold value below which interpolation starts to work. We specified σ_0 as 0.1 mN/m and n as 0.1 to magnify the effect of IFT-dependent relative permeability in contrast to the default σ_0 as 0.01 mN/m and n as 0.1.

We initially had expected a rising water cut behavior similar to the miscible CO_2 huff-n-puff case reported by Monger and Coma (1988) or observed in the Wolfcamp CO_2 huff-n-puff pilots. But as shown in Fig. 20, the water cut increase was minor despite considering different levels of relative permeability's dependency on IFT. One possible reason might be that only oil and gas phase relative permeability are treated as function of IFT, but the relative permeability to the water phase is not. Neither could the current model account for the dependency of water relative permeability on the water/oil or water/gas IFT. Hence future work on IFT-dependent water relative permeability might be required to further correlate the MMP with high water cut after CO_2 injection.

4.2.3. Reopening of water-bearing layers

Then we simulated the reopening of water-bearing layers (i.e., layer 9, 10, 11, and 12) by increasing the permeability of NF grid blocks from 0.025 mD (2.47×10^{-17} m^2) to 0.25 mD (2.47×10^{-16} m^2), on the assumption that natural fractures in these layers were reactivated due to gas injection. As shown in Fig. 21, the water cut did increase, but the increase was minor and the peak value was far lower than the observation from the field. Hence we do not recognize it as the major mechanism behind the surging water cut.

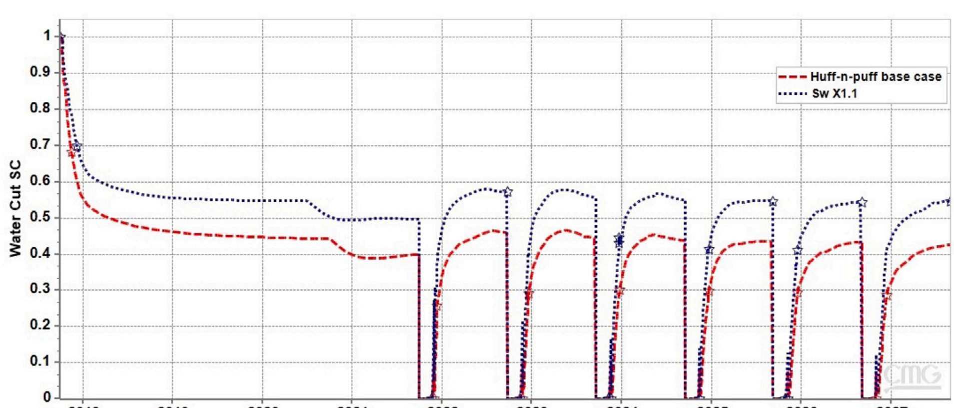

Fig. 19. Water cut response before and after increasing S_{wi}.

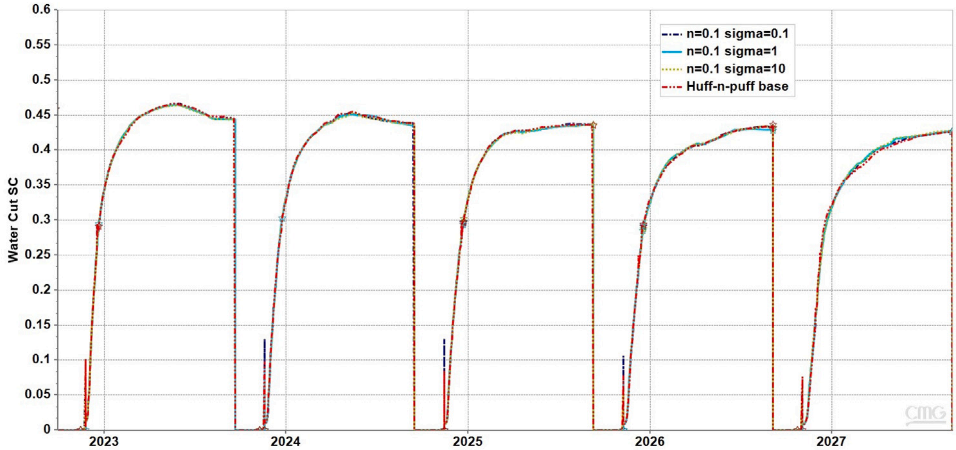

Fig. 20. Water cut responses with different levels of IFT-dependent relative permeability.

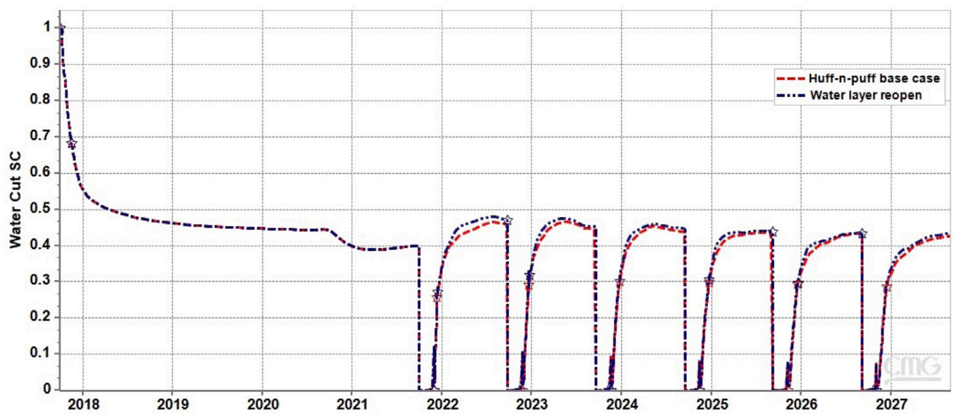

Fig. 21. Water cut response with and without the reactivation of NF in layer 9, 10, 11 and 12.

4.2.4. Reopening of unpropped hydraulic fractures

Previous studies (Chen et al., 2015; Ishida et al., 2016) have shown that the average breakdown pressure of supercritical CO_2 is only 73% of water due to its easier entrance into micro-fractures. The injected CO_2 will be in a supercritical state under the current injection pressure and in-situ temperature, and it might easily reopen the unpropped hydraulic fractures during huff-n-puff. The reopening of fractures during huff-n-puff can also be verified to some extent by the CO_2 breakthrough observed in the offset wells. CO_2 breakthrough was observed at the late time of injection under a high injection pressure, but its concentration level would return to normal once the injection stopped. Moreover, the severity of breakthrough could be reduced by elevating injection pressure in a step-wise manner, which strongly indicates such inter-well connectivity is mostly dominated by the reopening of preexisting fractures. Hence, we hypothetically changed the relative permeability curve of unpropped fractures from the matrix type, as shown in Fig. 8 to the fracture type, as shown in Fig. 9, assuming that unpropped hydraulic fractures were reopened due to CO_2 injection. Finally, we were able to obtain a relatively good match with field observations. As shown in Fig. 22, the water cut did increase due to the enhanced fractional flow of water, and it reached a maximum of 0.63. The water cut would gradually decrease with more cycles, but its value was still higher than the depletion base value as 0.39 which is close to the field observations. Fig. 23 exhibits the different recovery factors among depletion, huff-n-puff base and huff-n-puff with high water cut. It is obvious excessive water production is detrimental and would reduce the RF from 12.16% to 11.02%.

According to our simulation results, the most plausible reason behind the water cut surge is the reopening of unpropped hydraulic fractures. Hence, the future work will focus on managing water cut by a proper design of the operational constraints. For example, the maximum BHP for CO_2 injection stage must be tightly controlled in order to restrain the unpropped hydraulic fracture from reopening. Cyclic injection of hydrocarbon gas will also be investigated and then compared with the results with CO_2 injection in the future work.

5. Conclusions

A compositional modeling framework was established and implemented to investigate the reasons as well as the impact of the excessive water production during CO_2 huff-n-puff in tight oil reservoirs. To the best of our knowledge, it is the first time that such abnormal water cut behavior has been modeled for gas injection in tight oil reservoirs.

Fluid PVT and lab-scale model were established and tuned to match the experimental data, providing the critical inputs for the compositional model. A half-stage model of five fractures representing a typical well design in this region was then simulated as the base case, which demonstrated an improved oil RF from 7.96% of depletion to 12.16% after six cycles of CO_2 huff-n-puff. And the improvement factor as 1.53 matched the published results of gas IOR/EOR in unconventional reservoirs.

The literature review indicated several possible mechanisms including underestimation of initial water saturation, IFT-dependent relative permeability near miscibility, reactivation of water-bearing layers, and re-opening of unpropped hydraulic fractures. Our sensitivity studies based on the simulation identified the re-opening of unpropped hydraulic fractures as the most plausible reason for the water cut surge after CO_2 injection.

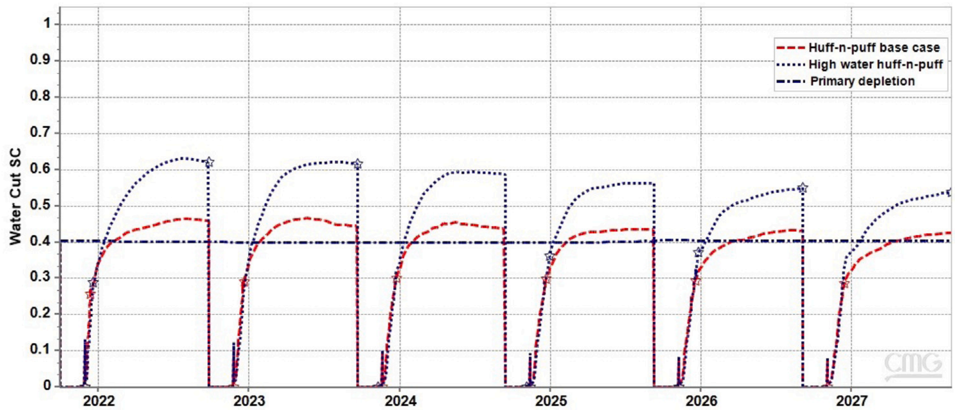

Fig. 22. Water cut response with and without reactivation of the unpropped HF.

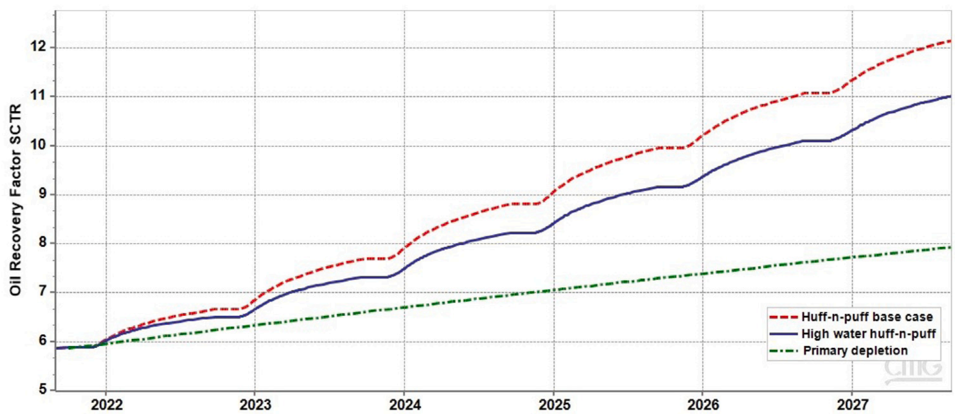

Fig. 23. Comparison of recovery factors among three representative cases.

Our simulation also found that the matched excessive water production would reduce the RF to 11.02% in contrast to 12.16% of the huff-n-puff base case, marking the water management as an important topic for future research.

CRediT authorship contribution statement

Chi Zhang: Writing - original draft, Investigation. **Ye Tian:** Conceptualization, Writing - original draft. **Yizi Shen:** Visualization. **Bowen Yao:** Writing - review & editing. **Yu-Shu Wu:** Writing - review & editing, Supervision.

Declaration of competing interest

The authors declare that they have no known competing financial interests or personal relationships that could have appeared to influence the work reported in this paper.

Acknowledgments

The authors would like to thank an anonymous industry partner for its financial and technical support of this work. Energi Simulation (formerly foundation CMG) and Computer Modelling Group are also acknowledged for supporting this study.

References

Abedini, A., Torabi, F., 2014. Oil recovery performance of immiscible and miscible CO_2 huff-and-puff processes. Energy Fuels 28 (2), 774–784.

Brown, M., Ozkan, E., Raghavan, R., Kazemi, H., 2011. Practical solutions for pressure-transient responses of fractured horizontal wells in unconventional shale reservoirs. SPE Reserv. Eval. Eng. 14 (06), 663–676.

Chen, C., Balhoff, M.T., Mohanty, K.K., 2014. Effect of reservoir heterogeneity on primary recovery and CO_2 huff'n'puff recovery in shale-oil reservoirs. SPE Reserv. Eval. Eng. 17 (03), 404–413.

Chen, Y., Nagaya, Y., Ishida, T., 2015. Observations of fractures induced by hydraulic fracturing in anisotropic granite. Rock Mech. Rock Eng. 48 (4), 1455–1461.

CMG, 2018. GEM User's Guide. Computer Modeling Group Ltd., Calgary, Canada.

Darvish, G.R., Lindeberg, E., Holt, T., Utne, S., 2006. Laboratory experiments of tertiary CO_2 injection into a fractured core. In: SPE/DOE Symposium on Improved Oil Recovery. Society of Petroleum Engineers.

Denoyelle, L., Lemonnier, P., 1987. Simulation of CO_2 huff'n'puff using relative permeability hysteresis. In: SPE Annual Technical Conference and Exhibition. Society of Petroleum Engineers.

EIA, 2020. U.S. crude oil production efficiency continues year-over-year improvements. https://www.eia.gov/todayinenergy/detail.php?id=42595. (Accessed 18 February 2020).

Haskin, H.K., Alston, R.B., 1989. An evaluation of CO_2 huff'n'puff tests in Texas. J. Petrol. Technol. 41 (02), 177–184.

Hawthorne, S.B., Gorecki, C.D., Sorensen, J.A., Steadman, E.N., Harju, J.A., Melzer, S., 2013. Hydrocarbon mobilization mechanisms from upper, middle, and lower bakken reservoir rocks exposed to CO_2. In: SPE Unconventional Resources Conference Canada. Society of Petroleum Engineers.

Hoffman, T.B., 2018. Huff-N-Puff gas injection pilot projects in the eagle ford. In: SPE Canada Unconventional Resources Conference. Society of Petroleum Engineers.

Hoffman, T.B., Evans, J.G., 2016. Improved oil recovery IOR pilot projects in the Bakken formation. In: SPE Low Perm Symposium. Society of Petroleum Engineers.

Hsu, H.-H., Brugman, R., 1986. CO_2 huff-puff simulation using a compositional reservoir simulator. In: SPE Annual Technical Conference and Exhibition. Society of Petroleum Engineers.

Ishida, T., Chen, Y., Bennour, Z., Yamashita, H., Inui, S., Nagaya, Y., Naoi, M., Chen, Q., Nakayama, Y., Nagano, Y., 2016. Features of CO_2 fracturing deduced from acoustic emission and microscopy in laboratory experiments. J. Geophys. Res. Solid Earth 121 (11), 8080–8098.

Jin, L., Hawthorne, S., Sorensen, J., Pekot, L., Bosshart, N., Gorecki, C., Steadman, E., Harju, J., 2017. Utilization of produced gas for improved oil recovery and reduced emissions from the Bakken formation. In: SPE Health, Safety, Security, Environment, & Social Responsibility Conference-North America. Society of Petroleum Engineers.

Kerr, E., Venepalli, K.K., Patel, K., Ambrose, R., Erdle, J., 2020. Use of reservoir simulation to forecast field EOR response-an eagle ford gas injection huff-n-puff application. In: SPE Hydraulic Fracturing Technology Conference and Exhibition. Society of Petroleum Engineers.

Kovscek, A.R., Tang, G.Q., Vega, B., 2008. Experimental investigation of oil recovery from siliceous shale by CO_2 injection. In: SPE Annual Technical Conference and Exhibition. Society of Petroleum Engineers.

Lai, S., Wardlaw, N., 1999. Factors affecting the application of anti-water coning technology (AWACT) at the south jenner oil field, southeast Alberta. J. Can. Petrol. Technol. 38 (03).

Li, L., Sheng, J.J., Su, Y., Zhan, S., 2018. Further investigation of effects of injection pressure and imbibition water on CO_2 huff-n-puff performance in liquid-rich shale reservoirs. Energy Fuels 32 (5), 5789–5798.

Li, L., Su, Y., Hao, Y., Zhan, S., Lv, Y., Zhao, Q., Wang, H., 2019. A comparative study of CO_2 and N_2 huff-n-puff EOR performance in shale oil production. J. Petrol. Sci. Eng. 181, 106174.

Luhning, R., Chmilar, M., Anderson, B., 1990. The AOSTRA anti water coning technology (AWACT) process-from invention to commercial application. In: Annual Technical Meeting. Petroleum Society of Canada.

Mohammed-Singh, L.J., Singhal, A.K., Sim, S.S.-K., 2006. Screening criteria for CO_2 huff'n'puff operations. In: SPE/DOE Symposium on Improved Oil Recovery. Society of Petroleum Engineers.

Monger, T., Coma, J., 1988. A laboratory and field evaluation of the CO_2 huff'n'puff process for light-oil recovery. SPE Res. Eng. 3 (04), 1–168.

Monger, T., Ramos, J., Thomas, J., 1991. Light oil recovery from cyclic CO_2 injection: influence of low pressures impure CO_2, and reservoir gas. SPE Res. Eng. 6 (01), 25–32.

Muirhead, M., Pettit, J., 2016. Permian Basin technical issues: (Part 1) How to manage water cut. https://ihsmarkit.com/research-analysis/permian-basin-technical-issues-part-1-how-to-manage-water-cut.html. (Accessed 10 December 2019).

Pan, H., Chen, Y., Sheffield, J., Chang, Y.B., Zhou, D., 2015. Phase-behavior modeling and flow simulation for low-temperature CO_2 injection. SPE Reserv. Eval. Eng. 18 (02), 250–263.

Pankaj, P., Mukisa, H., Solovyeva, I., Xue, H., 2018. Enhanced oil recovery in eagle ford: opportunities using huff-n-puff technique in unconventional reservoirs. In: SPE Liquids-Rich Basins Conference-North America. Society of Petroleum Engineers.

Sahni, V., Liu, S., 2018. Miscible EOR process assessment for unconventional reservoirs: understanding key mechanisms for optimal field test design. In: Unconventional Resources Technology Conference, Houston, Texas, 23–25 July 2018, Unconventional Resources Technology Conference. pp. 2907–2918.

Sanchez-Rivera, D., Mohanty, K., Balhoff, M., 2015. Reservoir simulation and optimization of Huff-and-Puff operations in the Bakken Shale. Fuel 147, 82–94.

Sheng, J.J., 2015. Enhanced oil recovery in shale reservoirs by gas injection. J. Nat. Gas Sci. Eng. 22, 252–259.

Simpson, M.R., 1988. The CO_2 huff'n'puff process in a bottomwater-drive reservoir. J. Petrol. Technol. 40 (07), 887–893.

Song, C., Yang, D., 2017. Experimental and numerical evaluation of CO_2 huff-n-puff processes in Bakken formation. Fuel 190, 145–162.

Sun, R., Yu, W., Xu, F., Pu, H., Miao, J., 2019. Compositional simulation of CO_2 Huff-n-Puff process in Middle Bakken tight oil reservoirs with hydraulic fractures. Fuel 236, 1446–1457.

Tang, G.Q., Aminzadeh, B., Zhou, D., Zhang, M., Lowry, D., Inouye, A., Song, S., Li, L., 2016. An experimental study on supercritical CO_2 injection in fractured tight reservoir to enhance oil recovery. In: Unconventional Resources Technology Conference, San Antonio, Texas, 1–3 August 2016, Unconventional Resources Technology Conference. pp. 602–618.

Tang, J., Smit, M., Vincent-Bonnieu, S., Rossen, W.R., 2019. New capillary number definition for micromodels: the impact of pore microstructure. Water Resour. Res. 55 (2), 1167–1178.

Teklu, T.W., 2015. Experimental and Numerical Study of Carbon Dioxide Injection Enhanced Oil Recovery in Low-Permeability Reservoirs (Ph.D. thesis). Colorado School of Mines. Arthur Lakes Library.

Tian, Y., Xiong, Y., Wang, L., Lei, Z., Zhang, Y., Yin, X., Wu, Y.S., 2019. A compositional model for gas injection IOR/EOR in tight oil reservoirs under coupled nanopore confinement and geomechanics effects. J. Nat. Gas Sci. Eng. 71, 102973.

Torabi, F., Asghari, K., 2010. Effect of operating pressure, matrix permeability and connate water saturation on performance of CO_2 huff-and-puff process in matrix-fracture experimental model. Fuel 89 (10), 2985–2990.

Tovar, F.D., Eide, O., Graue, A., Schechter, D.S., 2014. Experimental investigation of enhanced recovery in unconventional liquid reservoirs using CO_2: a look ahead to the future of unconventional EOR. In: SPE Unconventional Resources Conference. Society of Petroleum Engineers.

Vega, B., O'Brien, W.J., Kovscek, A.R., 2010. Experimental investigation of oil recovery from siliceous shale by miscible CO_2 injection. In: SPE Annual Technical Conference and Exhibition. Society of Petroleum Engineers.

Wang, Z., Ma, J., Gao, R., Zeng, F., Huang, C., Tontiwachwuthikul, P., Liang, Z., 2013. Optimizing cyclic CO_2 injection for low-permeability oil reservoirs through experimental study. In: SPE Unconventional Resources Conference Canada. Society of Petroleum Engineers.

Wang, L., Tian, Y., Yu, X., Wang, C., Yao, B., Wang, S., Winterfeld, P.H., Wang, X., Yang, Z., Wang, Y., Cui, J., Wu, Y.S., 2017. Advances in improved/enhanced oil recovery technologies for tight and shale reservoirs. Fuel 210, 425–445.

Yu, W., Zhang, Y., Varavei, A., Sepehrnoori, K., Zhang, T., Wu, K., Miao, J., 2019. Compositional simulation of CO_2 huff-n-puff in eagle ford tight oil reservoirs with CO_2 molecular diffusion, nanopore confinement, and complex natural fractures. SPE Reserv. Eval. Eng. 22, 492–508.

Zhang, K., 2016. Experimental and numerical investigation of oil recovery from Bakken formation by miscible CO_2 injection. In: SPE Annual Technical Conference and Exhibition. Society of Petroleum Engineers.